RANK-DEPENDENT CONTROL OF TUFT AND BEST4 CELL DEVELOPMENT IN THE INTESTINE

Reegan J. Willms[1,2,3], Tori McCabe[1,2], Lena Ocampo Jones[1], Ruth Schade[4] and Edan Foley[1,5]*.

1: Department of Medical Microbiology and Immunology, Faculty of Medicine and Dentistry, University of Alberta, Edmonton, AB, Canada

2: Equal contributions, author order selected randomly using the Siri function of EF's iPhone.

3: Current address: Department of Biological Sciences, MacEwan University, Edmonton, AB, Canada.

4: Department of Genetics, Stanford University, Stanford, CA, USA

5: Women and Children's Health Research Institute; Cancer Research Institute of Northern Alberta; Li Ka Shing Institute of Virology Department of Cell Biology, Faculty of Medicine and Dentistry, University of Alberta, Edmonton, AB, Canada.

ABSTRACT

Specialist intestinal epithelial cells are critical for barrier integrity and immune responses at the mucosal boundary, yet the pathways that govern their development are incompletely defined. Here, we identify an essential role for TNFRSF11A/RANK in shaping intestinal epithelial specialization in zebrafish. Using lineage trajectory analysis, we identified two tuft cell subtypes, including a subtype enriched for expression of genes required to produce pro-inflammatory leukotrienes. We showed that RANK deficiency reduced the abundance of type-2 tuft cells and BEST4 cells, increased goblet cell frequency, and promoted the accumulation of pro-inflammatory leukocytes in the gut. Functionally, we demonstrated that BEST4 cell numbers expand following infection with a pandemic strain of *Vibrio cholerae*, implicating this lineage in host defense against enteric pathogens. Together, our findings establish RANK as a critical determinant of epithelial diversification, linking loss of RANK to impaired epithelial immune regulation and an elevated inflammatory state.

INTRODUCTION

Specialist intestinal epithelial cells control host immunity at the mucosal boundary. For example, crypt-resident Paneth cells release antimicrobial factors that contribute to niche sterility, mucus-rich goblet cells maintain a physical barrier to microbial invasion, and M cells traffic luminal antigens to antigen-presenting cells in the lamina propria. More recent work suggests that a minimally characterized BEST4+ cell type may have important roles in the regulation of luminal pH and mucosal barrier hydration(1,2), potentially adding to the rich mosaic of epithelial cells that protect from infection.

Within the community of immune-modulatory epithelial specialists, tuft cells are a relatively rare type that are primarily known for involvement in type two immunity(3). Upon detection of luminal helminths, tuft cells activate ILC2s, which in turn release IL-4 and IL-13 to promote hyperplastic generation of tuft and goblet cells that support the capture and expulsion of helminths with the mucus barrier(4–6). Alongside established roles in type two immunity, recent studies uncovered involvement of tuft cells in antibacterial defenses(7), interactions with the commensal microbiome(8), and regeneration of damaged intestinal epithelia(9), indicating foundational involvement of tuft cells in gut function. However, despite the importance of tuft cells for intestinal health, we know relatively little about the signaling pathways that control tuft cell development.

In this study, we investigated the role of TNFRSF11A/RANK in the generation of immune-regulatory epithelial cells in zebrafish. RANK modifies epithelial development of several immunological structures(10), including the gut, where RANK is essential for M cell development(11–13). However, RANK also regulates gut remodelling during pregnancy(14); controls ILC3 activity(15); and drives tuft cell expansion in mice challenged with *Nippostrongylus brasiliensis*(16), pointing to an extensive involvement of RANK in shaping the epithelial barrier.

Zebrafish are an excellent system to characterize RANK-dependent control of intestinal epithelial development. The fish intestine houses epithelial, mesenchymal, and hematopoietic cells that mirror those found in mammalian guts(17,18), and there are striking similarities between the control of intestinal development in fish and mammals(19–22). Notably, we previously showed that RANK is expressed in larval

intestinal progenitor cells, and that commensal bacteria induce *rank* expression in progenitors and BEST4 cells(23), indicating possible unexplored roles for RANK in fish intestinal epithelial development.

Here, we present evidence that RANK is essential for development of tuft and BEST4 cells in the zebrafish gut, and that loss of RANK leads to an accumulation of goblet cells, and induction of pro-inflammatory states in gut-associated leukocytes. Functionally, we establish that BEST4 cells significantly increase in number after a natural infection with diarrheagenic *Vibrio cholerae*, confirming a role for BEST4 cells in navigating enteric infections. Combined our work indicates that RANK contributes to development of the intestinal epithelial barrier and demonstrates a role for BEST4 cells in host response to pathogenic bacteria in a live animal.

RESULTS

Zebrafish Intestines Contain Two Functionally Distinct Tuft Cell Types

In previous single cell gene expression atlases of zebrafish intestines(23,24), we identified a cluster of cells that expressed the definitive tuft cell marker *pou2f3* (Figure 1A-B). Upon re-examination, we discovered that the putative tuft cell population expressed multiple tuft cell markers, including tuft cell developmental regulators (*hmx2*, *sox9a*), genes associated with leukotriene synthesis (*alox5a* and *alox5ap*), and type two immune receptors (*il4r.1* and *il13ra1*) (Figure 1B). Like mammals, putative zebrafish tuft cells resolved into two distinct subtypes; one marked by expression of secretory gene products such as *arf1*, *sec22ba*, and *tmed2*, and a second subtype marked by expression of genes involved in immune responses to microbial patterns (Figure 1C-D). Of the two subtypes, the second expressed multiple genes involved in the production of pro-inflammatory leukotrienes (Figure S1), indicating that, like mammals, the zebrafish intestinal epithelium houses two tuft cell subtypes, including one linked to induction of type two defenses.

To explore regulators of tuft cell development, we used lineage trajectory analysis to visualize tuft cell maturation over pseudotime (Figure 1E). Both tuft cell subtypes mapped back to a similar undifferentiated cell state characterized by Notch pathway activity, including expression of *her6*, *her9*, and the HES5 ortholog, *her15.1* (Figure 1E-G). As cells progressed along the trajectories and Notch activity declined, we observed a spike in *pou2f3* expression that persisted in both lineages, followed by subtype-specific expression of the tuft-one marker *pdia2*, or the tuft-two marker *alox5a* (Figure 1F-G).

To track the abundance of the respective subtypes in the adult intestine, we performed fluorescence *in situ* hybridization assays for *pou2f3*, *pdia2*, and *alox5a* on sagittal intestinal sections of wildtype guts (Figure 1H). We found that, like mammalian intestines, fish tuft cells are relatively rare, accounting for approximately 2% of all intestinal epithelial cells (Figure 1I). We observed minimal co-expression of *alox5a* and *pdia2* (Figure 1I) and found that *alox5a*-positive cells preferentially accumulated at the villus base, while *pdia2*-positive cells distributed more evenly along the villus axis (Figure 1J), confirming that the respective genes marked two distinct cell types.

In addition to a putative *Notch-pou2f3-alox5a* trajectory, we were struck by early expression of the *tnfrsf11a*/*rank* gene during tuft cell development (Figure 1F-G). As *rank* marks the progenitor and tuft cell compartment of adult fish guts (Figure S2), and *rank* modifies epithelial development in other tissues, we characterized the relationship between expression of *her15.1*, *rank*, and *pou2f3* in wildtype intestines, and in a reporter line that expresses GFP under control of 3.4kb of DNA upstream of the *rank* start site, Tg(*rank:GFP*)(23). In both cases, we confirmed overlapping expression of *rank* with *her15.1* and *pou2f3* (Figure 1K-L), as well as enriched expression of the *rank:GFP* reporter in *pou2f3*-positive epithelial cells (Figure 1M-N). Notably, *pou2f3*, *rank:GFP* double-positive cells were frequently characterized by actin-rich bundles at the cell periphery, a hallmark of mature tuft cells(25,26) (Figure 1M, arrowhead).

Thus, in combination with our previous TEM-based identification of intestinal epithelial cells with classical tuft cell morphology(23), our work shows that the zebrafish intestine has two rare, functionally distinct tuft cell populations, including a specialist subtype that expresses type two immune receptors and genes required for production of pro-inflammatory leukotrienes.

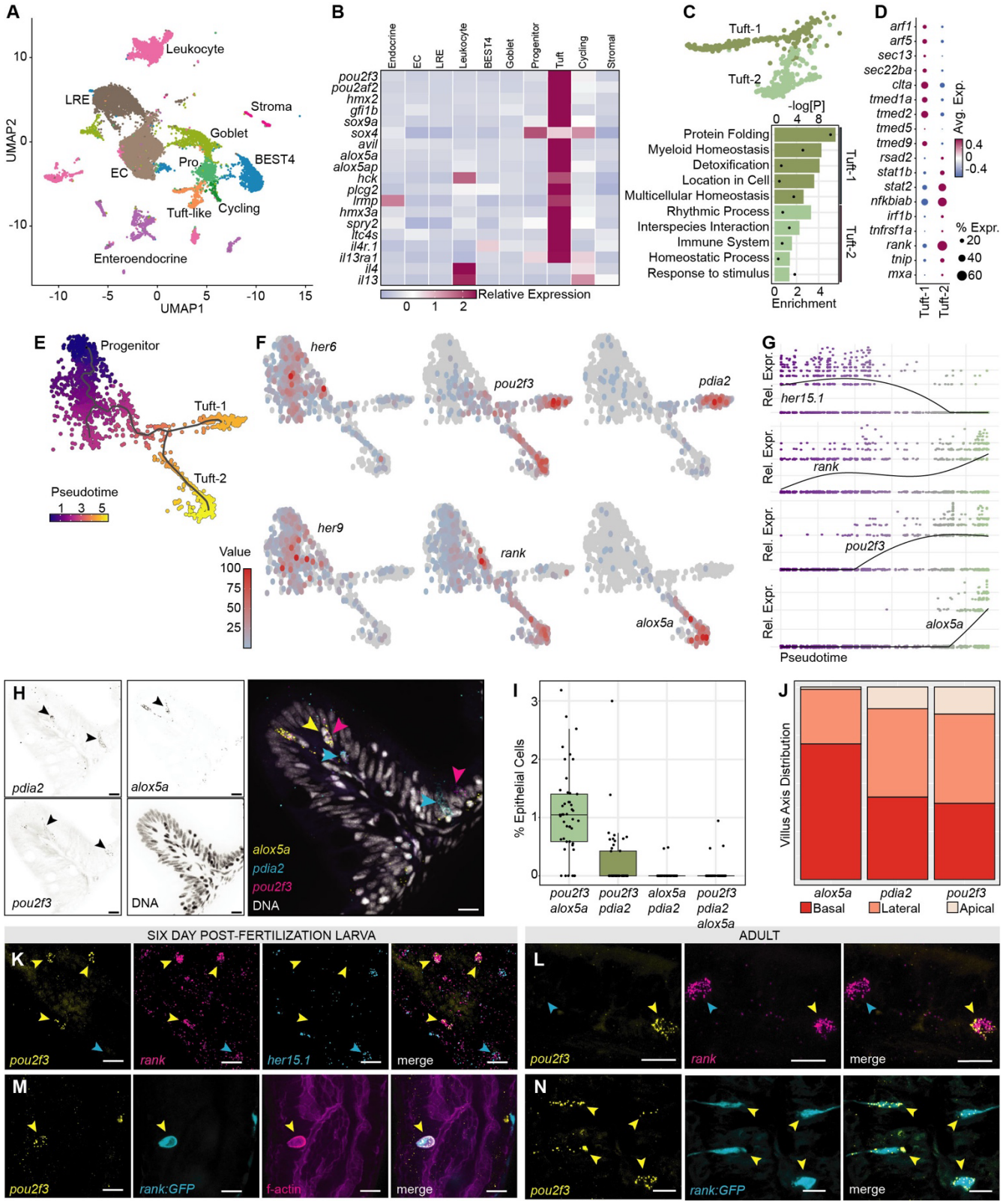

Figure 1. The Adult Zebrafish Has Two Tuft Cell Subtypes. A: UMAP representation of an adult single cell gene expression data set, indicating apricot-colored *pou2f3*-positive cells as "Tuft-like". **B:** Heatmap representation of the relative expression of tuft-related genes in the indicated cell types. **C-D:** Sub-clustering resolves two tuft cell subsets that express genes related to the indicated Gene Ontology terms (C) and express the indicated markers (D) In (C) fold-enrichment is indicated by bar length and negative log p-values with circles. In (D), heatmap

indicates scaled expression values. **E-G:** Visual representation of tuft cell maturation across pseudotime (E), including expression of the indicated marker genes (F-G). **H:** Fluorescence *in situ* hybridization showing the expression of the indicated genes in grayscale for each gene, and pseudo colored in the merged image. **I-J:** Percentage of intestinal epithelial cells that express the indicated markers (I), and position of the indicated cells along the villus axis (J). **K-N:** Visualizing expression of the indicated genes in wildtype (K-L), and Tg(*rank:GFP*, M-N) larval (K and M), and adult (L and N) zebrafish. In each image, scalebars are twenty micrometers, and arrowheads point to cells that express the gene of interest.

Rank is Necessary for Tuft Cell Development.

As *rank* expression marks a putative early tuft cell population (Figure 1E), we used CRISPR mutagenesis to better explore roles for RANK in gut development. To this end, we engineered a fish line with a five-nucleotide deletion in the third exon, generating a truncated protein with a frameshift at H58, followed by eight out of frame amino acids, and a premature stop codon (Figure 2A). The resulting protein lacks the C-terminal portion of the ligand binding domain, alongside the entire transmembrane and intercellular domains. Although homozygous viable, *rank* mutants were smaller than wildtype controls (Figure 2B), with significantly shorter intestines (Figure 2C), and impaired intestinal NF-κB activity (Figure S3). Homozygous *rank* mutants showed progressive symptoms of scoliosis with age (Figure S4), consistent with an essential role for RANK in osteoclast function(27). We found that *rank* deficiency abolished GFP expression in *rank:GFP* fish (Figure 2D-F), led to a significant loss of *pou2f3*-positive cells (Figure 2G), and a complete absence of actin-rich cells throughout the intestinal epithelium (Figure 2D, H), suggesting that RANK deficiency impacts the generation of mature tuft cells.

To better assess the impacts of RANK deficiency on gut function, we performed bulk RNA sequencing analysis of gene expression in intestines dissected from eight-week-old, co-housed, wildtype and *rank* mutant siblings derived from a heterozygous in-cross. Principal component analysis showed that *rank* mutant intestines were clearly distinct from wildtype counterparts (Figure 2I), with significant loss of expression of *rank* and *pou2f3* (Figure 2J), as well as disrupted expression of multiple genes linked with immune regulation (Figure 2K). To identify the intestinal cell types that are most sensitive to loss of *rank*, we mapped the fifty most significantly up and down-regulated genes in *rank* mutants to our adult single cell gene expression atlas(24). In this way, we discovered that greater than 70% of the most downregulated genes marked tuft cells, and 50% of the most

upregulated genes marked leukocytes (Figure 2L), suggesting impaired immune activity in RANK-deficient guts hallmarked by diminished tuft cell function, and enhanced hematopoietic cell activity.

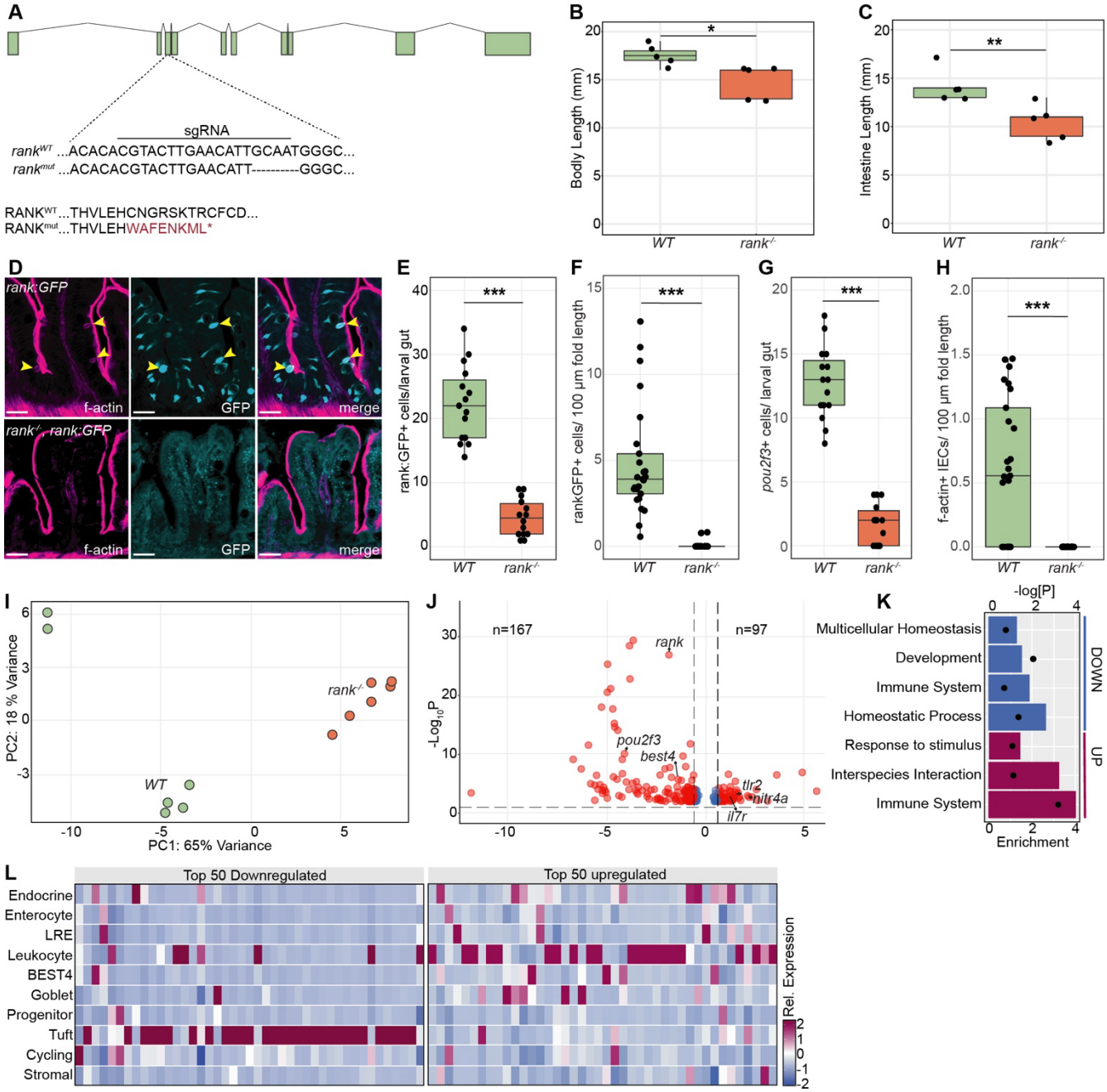

Figure 2. RANK Deficiency Impacts Intestinal Immunity. A: Schematic representation of the *rank* gene locus, with exonic DNA indicated in sage. The genomic region targeted by a RANK-directed sgRNA is indicated below, and the wildtype sequence alongside the mutated sequence is presented at the bottom. **B-C:** Body length (B), and intestinal (C) length of wildtype and RANK-deficient siblings. **D-H:** Visualization of filamentous actin (magenta) and GFP (cyan) in wildtype or *rank* mutant *rank:GFP* fish. The numbers of GFP+ cells per larval (E) and adult (F) guts are shown, as well as the number of f-actin rich (G) and *pou2f3*-positive (H) cells. **I-K:** Principal Component Analysis plot (I) of gene expression in wildtype and *rank* siblings. The volcano plot (J) shows

significantly differentially expressed (padj < 0.01) genes in mutants relative to wildtype fish, and the corresponding down and up-regulated gene ontology terms are shown in (K). Enrichment is indicated by bar length and negative log p-values with circles. **L:** Heatmap representation of the relative expression of the top 50 up and down-regulated genes in the indicated cell types. In each panel one asterisk = p<0.05, two = P < 0.01, and three = P < 0.001, calculated by ANOVA. In each image, scalebars are twenty micrometers, and arrowheads point to cells that express the gene of interest.

RANK Deficiency Causes Leukocyte Accumulation in the Gut.

As RANK modifies leukocyte-epithelium interactions(15,28), and loss of RANK deregulated the expression of immune effectors in the gut, we next characterized the consequences of RANK deficiency for the intestinal hematopoietic compartment. Here, we used our adult single cell gene expression atlas(24), to resolve the wildtype expression patterns of all leukocyte-associated genes that were dysregulated in *rank* mutants. Consistent with data in Figure 2L, the bulk of leukocyte-associated genes were expressed to higher levels in *rank* mutants than in their wildtype siblings (Figure 3A). We observed minimal induction of ILC2 activation markers in *rank* mutants, supporting a requirement for tuft cells in ILC2 activation (Figure 3B). Instead, we found that loss of RANK led to expression of pro-inflammatory markers in ILC3s (e.g. *nitr5*, and *ccl36.1*), macrophages (e.g. *mpeg1.1*, and *cxcl19*), B cells (e.g. *flt3*), and T cells (*il7r*) (Figure 3B-C). GO term analysis of all leukocyte-associated genes that are dysregulated in *rank* mutants confirmed that RANK deficiency switched leukocytes to an active, pro-inflammatory state, marked by elevated expression of genes required for leukocyte activation, antigen presentation, and immune effector functions (Figure 3D). To directly examine effects of RANK deficiency on gut-associated leukocytes, we stained sagittal sections of intestines prepared from co-housed eight-week-old wildtype and RANK-deficient siblings for the pan-leukocyte marker LCP-1 (Figure 3E-F). In this experiment, we consistently detected significantly enhanced recruitment of LCP-1-positive cells in *rank* mutant intestines relative to wildtype controls (Figure 3E-G). In sum, our work shows that loss of RANK results in an accumulation of intestinal leukocytes that express multiple activation markers, indicating that RANK-deficiency shifts the hematopoietic compartment to a pro-inflammatory state.

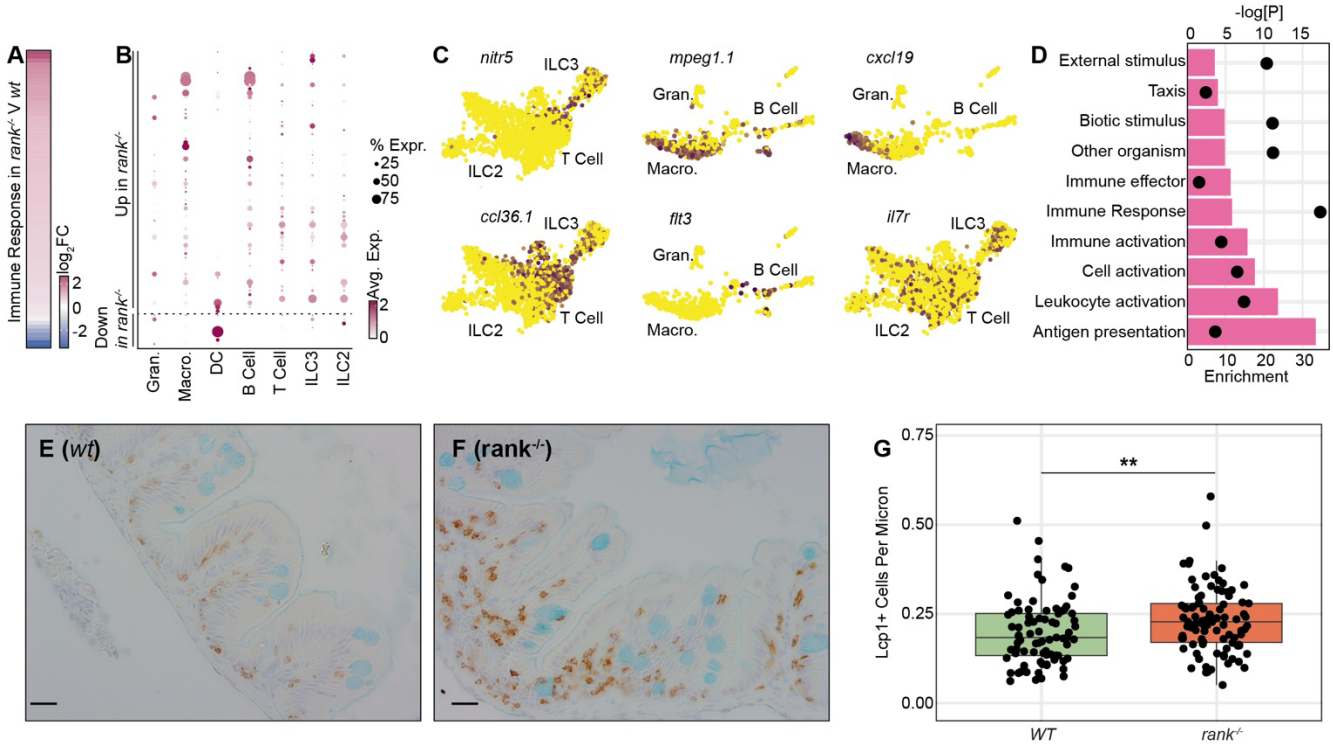

Figure 3. **RANK Deficiency Enhances Intestinal Infiltration by Activated Leukocytes: A-B:** Expression of all leukocyte-associated genes in *rank* mutants relative to wildtype siblings (A), and cell-type expression patterns of all each gene. **C:** Feature plots showing the leukocyte-specific distribution of the indicated set of genes with elevated expression in *rank* mutants. **D:** Gene ontology analysis of functions associated with all leukocyte-associated genes with enriched expression in *rank* mutants. Fold-enrichment is indicated by bar length and negative log p-values with circles **E-G:** Visualization (E-F) and quantification (G) of LCP-1-positive leukocytes in the intestines of wildtype (wt) and *rank* mutant siblings. Two asterisks = $P < 0.01$ calculated by ANOVA. Scalebars are twenty micrometers

RANK is Necessary for Development of *alox5a*-positive Tuft Cells

As RANK deficiency also impacted expression of tuft cell markers, we next used fluorescence *in situ* hybridization to visualize expression of *rank*, *alox5a*, and *pdia2* in anterior, middle, and posterior intestinal segments of eight-week-old wildtype (Figure 4A) and *rank* mutant siblings (Figure 4B). Consistent with our earlier data (Figure 2), we failed to detect *rank* transcript in *rank* mutant intestines (Figures 4A-B). In contrast, we observed subtype-specific impacts of RANK deficiency on the development of mature tuft cell subtypes. For example, whereas loss of *rank* led to a moderate decline in *pdia2*-positive type-one tuft cells exclusively in the intestinal anterior region, we discovered that RANK deficiency led to significant loss of *alox5a*-positive type-two tuft cells throughout all three intestinal epithelial segments (Figure 4C-E), indicating an intestine-wide

requirement for RANK in the development of immune regulatory tuft cells in the adult intestine, and a regionalized role for RANK in the specification of type one tuft cells in the anterior intestinal segment.

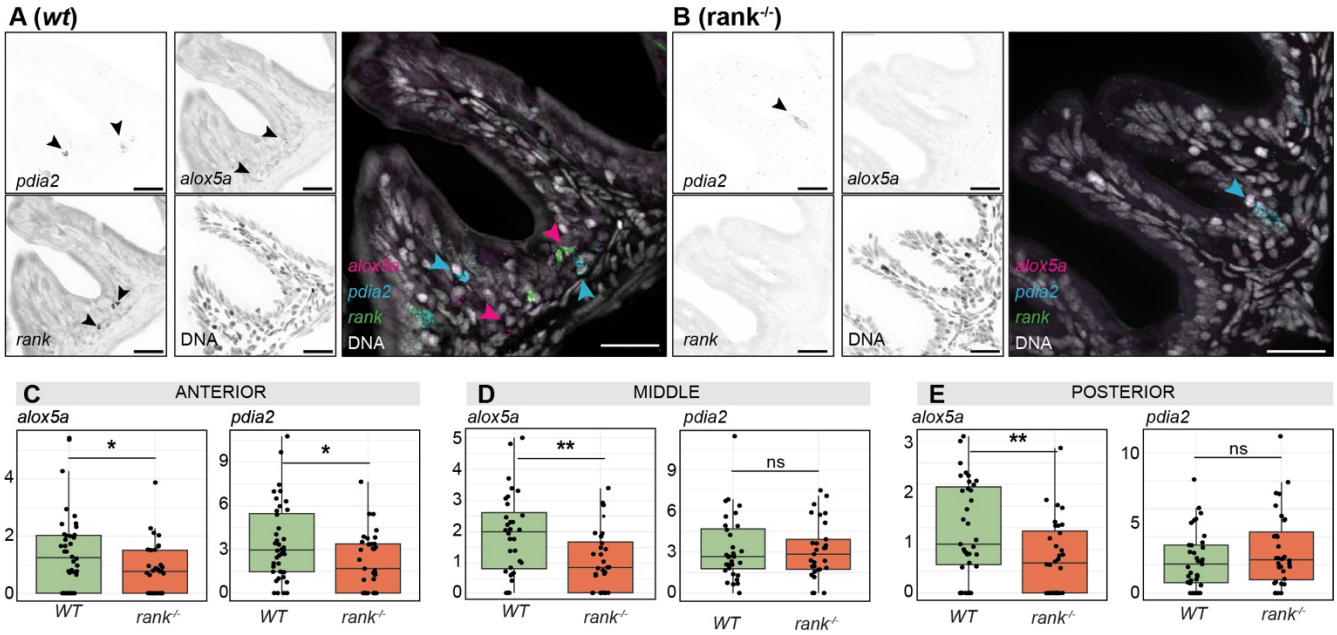

Figure 4. RANK Deficiency Results in Intestinal Loss of Type-2 Tuft Cells. A-B: Fluorescence *in situ* hybridization images of sagittal intestinal sections from wildtype (wt) and *rank* mutant siblings showing the expression of the indicated genes in grayscale for each gene, and pseudo colored in the merged image. **C-D:** Quantification of *alox5a* and *pdia2*-positive cells in anterior middle and posterior intestinal sections of wildtype (wt) and *rank* mutant siblings. In each panel one asterisk = p<0.05, and two = P < 0.01. In each image, scalebars are twenty micrometers, and arrowheads point to cells that express the gene of interest.

Loss of RANK Diminishes Expression of BEST4 Cell Markers.

Thus far, our work suggests that loss of RANK impedes homeostatic levels of type-2 intestinal tuft cells and leukocytes, two noted modifiers of gut immunity. However, we were also surprised by an unexpected decline in the expression of multiple BEST4 cell markers in *rank* mutants, including significantly reduced expression of definitive BEST4 cell markers such as *cftr*, *otop2*, and *best4* (Figure 5A). BEST4 cells have only been recently described but are common in the animal kingdom with the somewhat unexpected exception of mice(29), and we and others previously showed that larval and adult zebrafish intestines include related populations of BEST4 cells that express classical BEST4 cell markers(23,24,30,31), including guanylate cyclase 2C, ion channels, and carbonic anhydrases (Figure 5B). Through GO annotation of genes expressed in BEST4 cells from our larval and

adult single cell gene expression data sets, we found broad conservation of BEST4 cell function in larval and adult guts, with both populations expressing genes associated with development and immunity (Figure 5C).

We then used fluorescence *in situ* hybridization to determine the rostro-caudal and apico-basal distribution of BEST4 cells in the adult intestine (Figure 5D). We discovered that BEST4 cells were quite evenly distributed along the villus axis (Figure 5D). In contrast, we observed substantial differences for BEST4 cell distribution along the rostro-caudal axis. Although the frequency varied between experiments, we consistently observed the lowest frequency of cells in the posterior intestinal segment, where *best4*+ cells accounted for approximately 2% of all intestinal epithelial cells, relative to 3.5% in the anterior segment and 7.1% in the middle intestinal section. (Figure 5D). Our observation that *best4*+ cells exist at the base of fish villi contrasts with the predominately apical accumulation of BEST4 cells observed in human samples(1,32), and may reflect the fact that fish lack crypt-like structures in their intestines.

While BEST4 cells have been characterized as a distinct epithelial population, their relationship to other intestinal cell types remains unclear. To address this, we systematically compared BEST4 cell markers with those of all other adult gut cell types using Jaccard similarity, providing a quantitative measure of their relatedness (Figure 5E-F). Through a pairwise comparisons of marker gene expression across intestinal epithelial populations we identified three major transcriptional branches: immature progenitors; metabolically active LREs and enterocytes; and a secretory-associated branch that encompassed BEST4 cells along with the conventional goblet, tuft, and enteroendocrine secretory lineages. Notably, within the secretory-associated branch, BEST4 cells displayed the strongest transcriptional similarity to goblet and tuft cells, suggesting a closer relationship with these specialist cells (Figure 5E).

BEST4 cells express multiple genes involved in immune regulation (Figure 5C, Figure S5), and BEST4 cells are sensitive to diarrhea-causing bacterial toxins in human intestinal organoids(33). However, there are no *in vivo* data on the sensitivity of BEST4 cells to diarrheagenic pathogens. Therefore, we tested the effects of a *Vibrio cholerae* (*Vc*) infection on BEST4 cell populations in the adult intestine. We selected *Vc*, as zebrafish are susceptible to natural infections with *Vc*(34), and BEST4 cells are marked by expression of the ion channel *cftr*

that initiates the massive chloride efflux responsible for diarrheal disease in cholera. To determine the impact of *Vc* on BEST4 cells, we enumerated *cftr*-positive cells in intestines of zebrafish that we challenged with *Vc* for 24h, followed by a one- or five-day recovery period (Figure 5G-I). In these experiments, we discovered that exposure to *Vc* led to a significant increase in the number of *cftr*-positive intestinal epithelial cells at both time points (Figure 5J), establishing an *in vivo* sensitivity of BEST4 cells to diarrheagenic bacteria. Combined, our data indicate that BEST4 cells are a widespread, pathogen-sensitive cell type in the adult intestinal epithelium, with gene expression profiles that indicate possible roles in epithelial defenses.

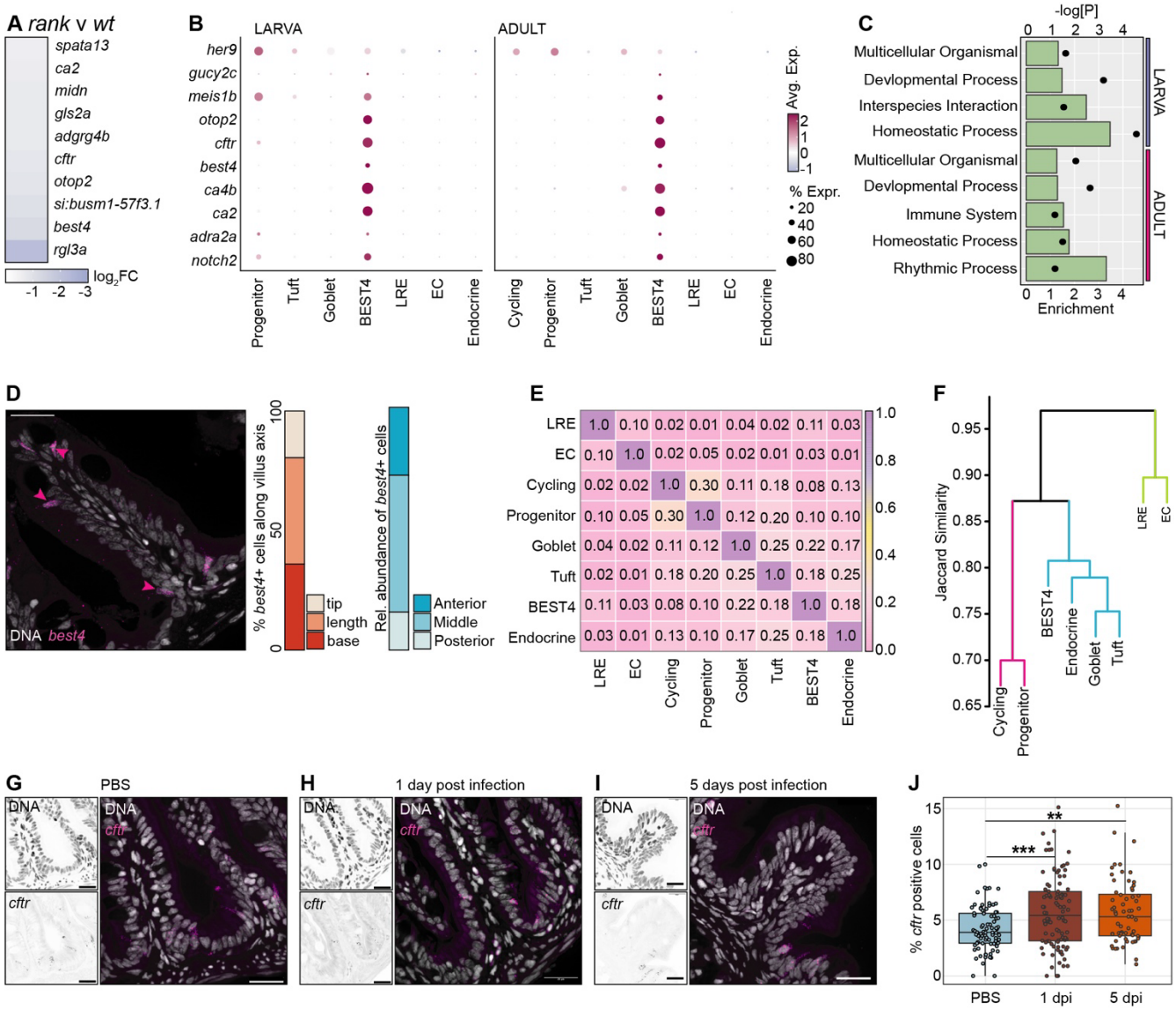

Figure 5. The Adult Zebrafish Intestine Contains BEST4 Cells that Respond to Infection with *Vibrio cholerae*. A-B: Expression of BEST4 cell marker genes in *rank* mutants relative to wildtype siblings (A), and cell-type expression

patterns of established BEST4 cell markers in larval and adult intestines (B). **C:** Gene ontology analysis of terms associated with markers of larval and adult BEST4 cells. Enrichment is indicated by bar length and negative log p-values with circles. **D:** Representative fluorescence *in situ* hybridization image of *best4+* cells (magenta) in the adult zebrafish intestine. Bar charts show the relative distribution levels of BEST4 cells along the villus axis (red shades), and the relative abundances of *best4+* cells in the anterior, middle, and posterior segments (blue shades). **E-F:** Jaccard similarity analysis of genes expressed in the respective cell types. **G-I:** Fluorescence *in situ* hybridization images of sagittal intestinal sections from wildtype adult zebrafish showing the expression of *cftr* (magenta) in control fish (G), or *Vc*-infected fish that were give one (H) or five (I) days to recover from infection. **J:** Quantification of *cftr*-positive cells in intestines of the indicated treatment groups. In each panel two asterisks = $p<0.01$, and three = $P < 0.001$. In each image, scalebars are twenty micrometers, and arrowheads point to cells that express the gene of interest.

RANK is Necessary for BEST4 Cell Development

As RANK deficiency impacted expression of multiple BEST4 cell markers, we examined the effects of *rank* mutation on BEST4 cells. The 2F11 antibody labels cells positive for Annexin A4 (Anxa4), a gene predominantly expressed in the BEST4/secretory cell population (Figure 6A). We used immunofluorescence to confirm the existence of Anxa4-positive cells throughout the intestinal epithelium of *rank:GFP* adults, including in GFP-positive cells (Figure 6B), and we showed that loss of RANK significantly diminished the number of Anxa4-positive cells along the villus axis (Figure 6B-C), confirming an essential role for RANK in the development of Anxa4-positive cells. As Anxa4 marks multiple mature cell types, we systematically determined the consequences of RANK deficiency for goblet cells, enteroendocrine cells, and BEST4 cells throughout the intestinal epithelium.

Loss of RANK did not diminish expression of any of twenty goblet cell marker genes (Figure 6D) or lower the number of intestinal epithelial goblet cell numbers (Figure 6E). Instead, we observed a significant increase in the number of Alcian blue-positive goblet cells in *rank* mutants, relative to their wildtype sibling controls (Figure 6E-F). We view the inverse relationship between goblet cell numbers and BEST4 cell numbers as potentially interesting, given reports that BEST4 cells and goblet cells are often found in pairs(35,36), and that treatment of mouse small intestinal organoids with RANK ligand enhances expression of goblet signature genes(37). Unlike tuft and goblet cells, RANK deficiency had minimal effects on enteroendocrine cell numbers, only affecting the representation of *neurod1*-positive enteroendocrine cells in the posterior intestinal epithelium (Figure 6G-H). In contrast, we found that RANK deficiency significantly impacted BEST4 cell numbers throughout the intestinal epithelium, leading to a greater than 50% drop in BEST4 cell numbers in each section (Figure 6G, I).

Combined, our results uncover an epithelium-wide role for the zebrafish *rank*/*tnfrsf11a* ortholog in the development of intestinal epithelial type-two tuft cells and BEST4 cells, and a restricted requirement for RANK in the development of posterior enteroendocrine cells and anterior intestinal type one tuft cells.

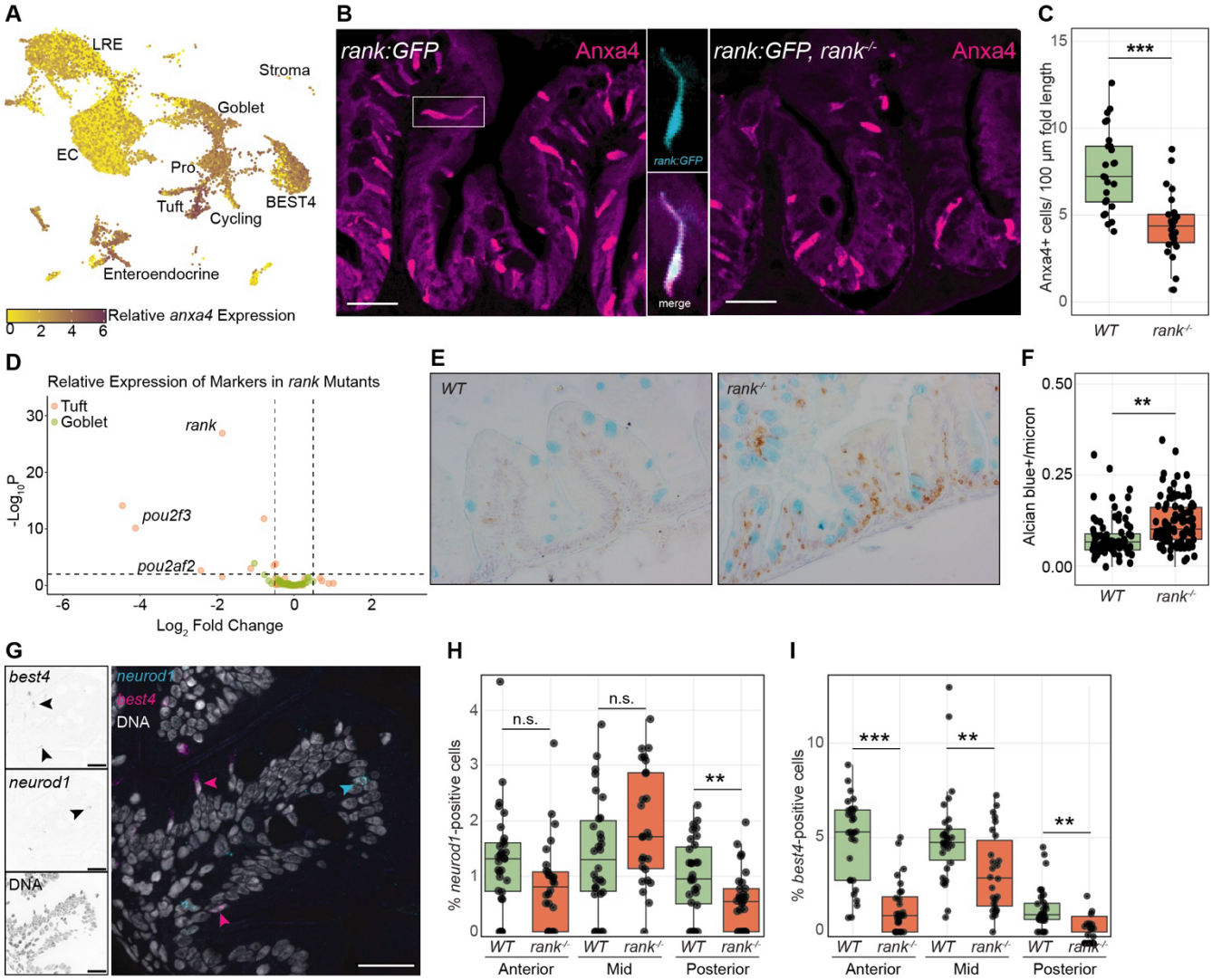

Figure 6. RANK Deficiency Leads to Epithelium-Wide Decrease in BEST4 Cell Numbers. Feature plot showing the relative expression of the 2F11 antibody target *anxa4* in the adult intestine. **B:** Visualization of Anxa4+ positive cells (magenta) in wildtype or RANK-deficient *rank:GFP* adult fish. Boxed region indicates a single GFP, Anxa4 double-positive cell in the merged image. **C:** Quantification of Anxa4-positive cells in wildtype and *rank* mutant intestines. Relative differential expression of the top 20 goblet cell (sage) and tuft cell (apricot) markers in *rank* mutants relative to wildtype controls. **D-E:** Visualization (D) and quantification (E) of Alcian blue-positive goblet cells in wildtype and *rank* mutant adults. Both images were counterstained with the leukocyte marker Lcp-1 (brown) to assist orientation of samples. **F:** fluorescence *in situ* hybridization images of sagittal intestinal sections from wildtype fish showing pseudo colored expression of the BEST4 cell marker *best4* and the enteroendocrine cell marker *neurod1* in a representative wildtype intestine. **G-H:** Quantification of *neurod1* (H) and *best4* (I)-positive epithelial cells in the anterior, middle, and posterior intestinal segments of wildtype and *rank* mutant

intestines as indicated. In all panel, two asterisks = $P < 0.01$, and three = $P < 0.001$, calculated by ANOVA. In each image, scalebars are twenty micrometers, and arrowheads point to cells that express the gene of interest.

DISCUSSION

At the intestinal barrier, specialized cells harvest nutrients, protect from pathogens, and coordinate tolerant immune responses to the resident microbiota. As epithelial breaches fuel inflammatory disease, it is essential that we decipher the pathways responsible for barrier formation and maintenance. RANK has critical roles in the mammalian intestine, where it controls M cell development(11,13), epithelial remodelling during pregnancy(14), ILC3 activity(15), and antiparasitic defenses(16). However, we know less about effects of RANK deficiency on homeostatic maintenance of the gut epithelium. In this study, we determined the consequences of RANK deficiency for the adult zebrafish gut. We found that loss of RANK diminished the epithelial abundance of type two tuft cells and BEST4 cells and showed that RANK deficiency led to an accumulation of goblet cells and pro-inflammatory leukocytes, suggesting that RANK is critical for immune homeostasis in the adult gut. Moving forward, we feel our work raises several questions that merit investigation.

How do zebrafish tuft cells relate to mammalian equivalents? As zebrafish intestines contain ILC2s and ILC3s(38), and fish encode immune-regulatory *il-4*, *il-13*, and *il-10* orthologs(39,40), we view zebrafish as an excellent animal to characterize type two immunity. Mammalian tuft cells are a relatively rare post-mitotic secretory lineage that activates antiparasitic defenses(41), contributes to antibacterial immunity(7), and provides a reserve population of stem cells for injury-dependent tissue regeneration(9). However, prior to this study, tuft cells had not been unambiguously identified in the adult fish gut. We found that, like mammals, zebrafish intestines contain two *pou2f3*-positive actin-rich tuft cell subtypes, including one marked by expression of receptors for IL-4 and IL-13, and genes required for production of pro-inflammatory leukotrienes, indicating the existence of specialist fish tuft cells dedicated to type two defenses. Our work indicates that RANK is necessary for development of type two tuft cells along the entire rostro-caudal axis of the gut. However, our work also indicates noteworthy differences between fish and mammalian tuft cells. In mice, tuft cell-derived IL-25 is essential for tuft cell-dependent induction of type two immunity(5–7,42,43). As the fish genome does not appear to encode an *il-25* ortholog, it is unclear if, or how, fish tuft cells engage neighboring ILC2s. However, we note that intestinal tuft cells from humans and non-human primates also do not appear to appear to express IL-

25(44,45). Thus, we consider it possible that additional mediators of tuft cell-ILC2 communication require identification. Perhaps the most striking difference between fish and mammalian tuft cells is the apparent absence of *choline acetyl transferase* expression in fish tuft cells. In mammals, acetylcholine is a prominent effector of tuft cell-dependent immunity(46), including direct effects on helminth fecundity(47), suggesting that fish tuft cells may rely on a distinct class of effectors to protect from infection. In the future, it will be of interest to determine the impacts of fish tuft cells on antiparasitic immunity in live infection models.

What is the relationship between tuft cells, BEST4 cells, and goblet cells? We often view development of mature intestinal epithelial cells as a metronomic progression through maturation states that are controlled by germline-encoded signaling pathways. However, epithelial maturation is a more stochastic event that is also dictated by damaging agents, pathogen-derived virulence factors, or metabolic products of commensal bacteria. For example, luminal parasites promote accumulation of tuft and goblet cells that initiate the "weep and sweep" elimination of the parasite(4–6), while commensal bacteria promote a growth in goblet cell numbers and a thickening of the mucus barrier(48,49). Our work suggests that BEST4 cells are part of this plastic community of microbe-sensitive intestinal epithelial cells. From a transcriptional perspective, we find that BEST4 cells are most like secretory cell types with the closest relationship to goblet and tuft cells, and we present evidence that RANK deficiency affects the epithelial abundance of type two tuft cells, BEST4 cells, and goblet cells. Our findings match data that tuft and BEST4 cells share a common progenitor in rats(50), and align with reports that exposure of mouse small intestinal organoids to RANK ligand enhances expression of tuft signature genes(16) and suppresses expression of goblet cell signatures(37). In agreement with data from human intestinal organoids(33), we find that *Vibrio cholerae* promote accumulation of BEST4 cells in the fish gut, demonstrating that BEST4 cells are sensitive to encounters with diarrheagenic pathogens *in vivo*, and supporting a role for BEST4 cells in sensing and responding to luminal microbes. In the future, it will be valuable to identify the factors responsible for development of BEST4 and secretory lineages in the presence or absence of pathogenic challenges.

How do BEST4 cells relate to M cells? In mammals, RANK is essential for M cell development(11,51). As fish intestines do not appear to include M cells, we cannot chart the developmental relationships between M cells

and BEST4 cells in the fish gut. However, our finding that RANK deficiency leads to a loss of BEST4 cells matches a report that human BEST4 cell development proceeds through a transient M-like cell state(1). In contrast, recent work with human intestinal organoids showed that treatment with RANK ligand led to a loss of BEST4 cells, and a concomitant gain of M cells, suggesting differential effects of RANK signaling on BEST4 and M cell development(33). We speculate that the opposing effects of RANK ligand exposure on BEST4 and M cell maturation in organoids may reflect the difficulty of formulating a growth medium that permits simultaneous development of both cell types.

Are BEST4 cells involved in intestinal epithelial defenses? First described in a histological study of human intestinal epithelial cells(35), BEST4 cells were subsequently profiled in single cell gene expression atlases that showed BEST4 cells express ion channels, such as *best4* and *cftr*, alongside carbonic anhydrases needed for acid-base homeostasis, pointing to possible roles for BEST4 cells in mucus hydration and luminal pH(1,2,32,44,52,53). At the same time, patient data implicated BEST4 mutations in poor colorectal cancer prognosis(54), underscoring a need to understand how BEST4 cells function *in vivo*. Since their identification in humans, BEST4 cells have been found in zebrafish(23,24,30,31), macaques(55), pigs(56), rabbits(29), pythons(57), and rats(50), suggesting an evolutionarily conserved role for BEST4 cells in gut function. Given their physical proximity to goblet cells, their putative roles in pH regulation and mucus hydration, and their sensitivity to enteric pathogens, we hypothesize that BEST4 cells may contribute to the regulation of host-microbe interactions in the gut. In this regard, we consider it particularly intriguing that zebrafish BEST4 cells express elevated levels of the prostaglandin *ptger4c* receptor(31), as well as the leukocyte chemokine *ccl25a*(24). As mice intestines lack BEST4 cells, we believe zebrafish are an ideal animal model to explore roles for BEST4 cells in host responses to commensal and pathogenic microbes.

As a caveat, we note our study characterized intestinal physiology in a mutant that simultaneously affected the epithelial representation of three cell types: tuft cells, BEST4 cells and goblet cells. As a result, our work does not allow us to make any inferences related to the developmental relationships of the respective cell types. For example, it is possible that BEST4 and tuft cells share a common progenitor, but it is equally possible that loss of

one cell type indirectly affects the abundance of the other. Moving forward, it will be of interest to identify the signaling networks responsible for the developmental specification of the respective lineages.

MATERIALS AND METHODS

Animal Husbandry and zebrafish lines

All zebrafish experiments were approved by the University of Alberta's Animal Care & Use Committees of Biosciences and Health Sciences (AUP#3032), operating under the guidelines of the Canadian Council of Animal Care. Wild type TL, Tg(*rank:GFP*), and Tg(*NFkB:GFP*) were reared at 27°C in facility water (Instant Ocean Sea Salt dissolved in reverse osmosis water maintained at a conductivity of 1000µS and pH buffered to pH 7.0 with sodium bicarbonate) under a 14h/10h light/dark cycle using standard zebrafish husbandry protocols. Embryos raised to larvae were housed at 29°C under a 14h/10h light/dark cycle.

Generating rank mutants

Tg(*rank*:GFP) was described previously(23). To generate rank mutants, CRISPR-Cas9 mutagenesis was carried out as described previously(58) using the IDT AltR CRISPR-Cas9 System. Briefly, the cytoplasm of single-celled Tg(*rank:GFP*) embryos were injected with approximately 1nL of 5µM gRNA:Cas9 ribonucleoprotein complex: duplexed gRNA, trans-activating crispr RNA (tracrRNA; IDT 1072533), and Cas9 enzyme (IDT) in IDT duplex buffer (IDT 11-05-01-03). To generate stable mutants, injected embryos were reared to adulthood, then single adults were outcrossed to AB wild-type fish. F1 progeny were reared, in-crossed and genotyped by fin clipping to search for F2 generations bearing a frame-shift mutation. PCR amplicons were generated with the following primers: rank diagnostic forward primer CACACACGCACATGAACTATAACC; rank diagnostic reverse primer GTCTTAAAGTGACACGAACCC. Cutting efficiency was assessed by PCR and amplicon digestion with the restriction enzyme MslI (NEB R0571L), where lack of digestion indicated disruption of the recognition sequence. Amplicons were sequenced at the Molecular Biology Services Unit at the University of Alberta to determine the nature of the lesion.

Generating rank crispants in Tg(*NF-kB*:EGFP) background

To investigate the effect of *rank* activity on NF-kB:EGFP, single cell-stage NF-kB:EGFP embryos were injected with Cas9 enzyme (control, no sgRNA) or Cas9 enzyme complexed with *rank* sgRNA to generate *rank* crispants. At 6 days post fertilization, the larvae were euthanized with tricaine, fin clipped, genotyped and fixed overnight at 4°C. Larvae were washed three times with PBS then embedded in 0.7% UltraPure low melting point agarose (Invitrogen Cat#16520) on a glass bottom dish.

HCR™ RNA Fluorescence *in situ* hybridization

Molecular Instruments Multiplexed HCR™ RNA-FISH (v3.0) protocol for Fresh/Fixed Frozen Tissues was followed to detect mRNA of interest in adult intestinal tissue sections (5µm thickness) and has been described previously(24). HCR-RNA FISH probes used in this paper were *alox5a*, *best4*, *cftr*, *her15.1*, *neurod1*, *pdia2*, *pou2f3*, and *tnfrsf11a* (*rank*).

Immunofluorescence

Zebrafish intestines were fixed in 4% paraformaldehyde (diluted in PBS from a 16% stock: EMS Cat#15710) overnight at 4°C. Intestines were washed twice in 1xPBS then cryoprotected in 15% (w/v) sucrose/PBS at room temperature until sunk followed by sinking in 30% (w/v) sucrose/PBS (overnight at 4°C). Intestines were mounted in optimal cutting temperature embedding medium (Fisher Scientific Cat #23-730-571), then frozen on dry ice. Five micrometer sections were collected on Superfrost Plus slides (Fisherbrand Cat #22-037-246). After allowing sections to adhere onto slides, slides were immersed in PBS for 20 minutes at room temperature. Tissue was blocked for 1h at room temperature in 3% (w/v) Bovine Serum Albumin dissolved in PBST (1xPBS + 0.2% (v/v) Tween-20). Primary antibodies were diluted in blocking buffer then layered onto sections. Sections were incubated in primary antibody solution overnight in a humid chamber at 4°C. Excess primary antibody was washed by immersing slides in fresh PBST for 1.5h. Sections were incubated in secondary antibody solution for 1h at room temperature in a humid chamber, protected from light. All secondaries were prepared at a 1:2000 dilution in blocking buffer; Phalloidin was added to the secondary antibody solution at 1:500. Secondary solution was removed then sections incubated in Hoechst diluted 1:2000 in PBST for 10 minutes protected from light.

Slides were washed in PBST by brief immersion followed by a 30-minute incubation in fresh PBST protected from light. Slides were mounted in Fluoromount™ Aqueous Mounting Medium (Sigma F4680-25mL). Primary antibodies used for immunofluorescence in this study: Chicken polyclonal anti-GFP (ThermoFisher Scientific Cat# PA1-9533) at 1:1000; Mouse anti-zebrafish gut secretory cell epitopes (abcam Cat# ab71286) at 1:500. Fluorescent secondaries and stains used in this study were: Goat anti-chicken IgY (H+L) secondary antibody, Alexa Fluor™ 488 (ThermoFisher Scientific Cat# A-11039); Goat anti-Rabbit IgG (H+L) Cross-Adsorbed Secondary Antibody, Alexa Fluor™ 568 (ThermoFisher Scientific Cat# A-11011); Alexa Fluor™ 647 Phalloidin (ThermoFisher Scientific Cat# A22287); Hoechst 33258 (Molecular Probes Cat #H-3569).

Lcp1 Immunohistochemistry & Alcian blue staining

Heterozygous Tg(*rank:GFP*); *rank* +/- were in-crossed and progeny co-housed. At 7 weeks post fertilization, the progeny were genotyped then five fish per genotype (rank +/+ and rank -/-) were co-housed until 10 weeks post fertilization. Experimental fish were fasted for 24h prior to dissection. Whole intestines from 10-week-old fish were dissected then fixed overnight at 4°C in BT fixative (4% PFA, 0.15mM CaCl2, 4% sucrose in 0.1M phosphate buffer pH 7.4). Whole intestines were processed for paraffin embedding at the University of Alberta Biological Sciences Advanced Microscopy Facility then IHC performed on 5µm tissue sections as described previously(24). L-Plastin was detected in 10-week-old intestines using rabbit anti-Lcp1 antibody (GeneTex GTX124420, 1/10000) followed by colorimetric detection using Cell Signaling Technology® SignalStain® Boost Detection Reagent HRP Rabbit (Cat 8114) and SignalStain® DAB Substrate Kit (Cat 8059, 10 minutes). Slides were then stained with Alcian blue for 3 minutes followed by a 10-minute rinse in running tap water. Nuclei were counterstained with ¼-strength hematoxylin (30 seconds) followed by another 10-minute rinse in running tap water. Tissue was then dehydrated, cleared with toluene, and mounted in Dpx. The fish used in this experiment were also used to measure body length and whole intestine length.

Microscopy

Histological samples were imaged on a ZEISS AXIO A1 compound light microscope with a SeBaCam 5.1MP camera. Confocal images of intestinal tissue sections were captured on an Olympus IX-81 microscope fitted with a CSU-X1 spinning disk confocal scan-head, Hamamatsu EMCCD (C9100-13) or Hamamatsu Orca-Fusion BT digital sCMOS camera and operated with PerkinElmer's Volocity. Whole larval confocal imaging was performed on a Leica Falcon SP8 equipped with a 25x 0.95NA Water HC Fluotar objective lens then stitched with Leica Application Suite X software. Fiji(59) was used to generate maximum intensity projections of confocal Z-stacks and false color manipulations.

Bulk RNAseq of whole intestines

Heterozygous Tg(*rank:GFP*); rank +/- were in-crossed and progeny co-housed. At 7 weeks post fertilization, the progeny were genotyped then six fish per genotype (rank +/+ and rank -/-) were co-housed until 8 weeks post fertilization. Experimental fish were fasted for 24h prior to dissection for RNA extraction. Whole intestines from 8-week-old fish were dissected then homogenized in Trizol Reagent then RNA was extracted following manufacturer's suggestions. Fish carcasses were fin clipped and genotyped by Sanger sequencing. Pure RNA was sent to Novogene for polyA enrichment of the RNA library (unstranded) and sequencing on NovaSeq X Plus (PE150, Q30≥85%)(6Gb raw data per sample).

Bulk RNA-Seq quality control and alignment

The fastq files were processed using the default parameters of the nf-core RNA-seq pipeline (version 3.9)(60,61). Quality control metrics were assessed via FASTQC (version 0.11.9). Adaptors and low-quality reads were filtered out using the default parameters of TrimGalore! (version 0.6.7). STAR (version 2.7.10a) was used to map reads to the zebrafish genome (GRCz11). Salmon (version 1.5.2) quantified transcripts(62).

Bulk RNA-Seq data processing and DESeq2 analysis

The quantification files produced by Salmon were used for further analysis with the DESeq2 (version 1.38.3) R package(63), which also assigned Zebrafish Information Network symbols to each gene. Differential expression analyses were completed with DESeq2 to identify genes differentially expressed between wild type and *rank*$^{-/-}$ fish, with an adjusted *p*-value < 0.01 considered significant. Significantly differentially expressed genes were then used for principal component analysis, which was also completed with DESeq2.

SUPPLEMENTARY FIGURES

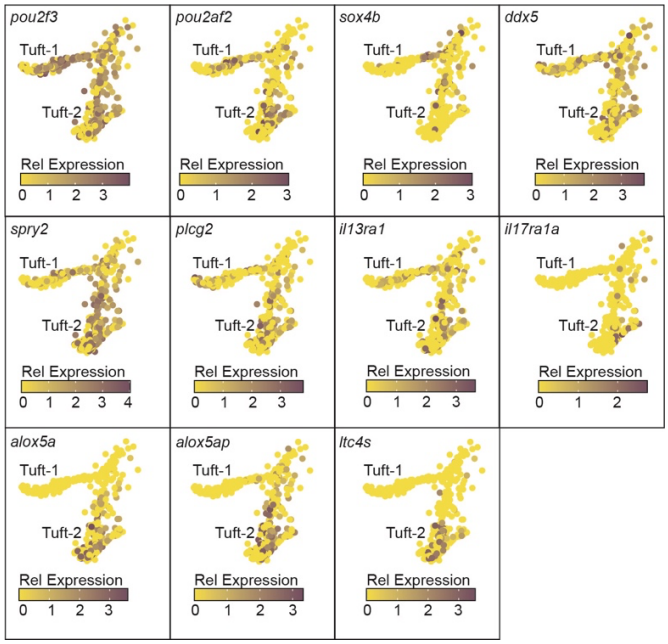

Figure S1. Expression of classical tuft cell markers (panels from *pou2f3* to *plcg2*) and immune regulatory markers (panels from *il13ra1* to *ltc4s*) in zebrafish tuft cells.

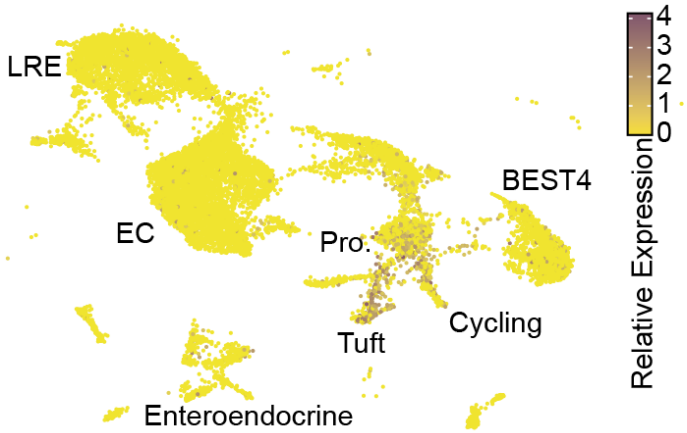

Figure S2. Feature plot showing expression of *rank* in the adult intestinal epithelium.

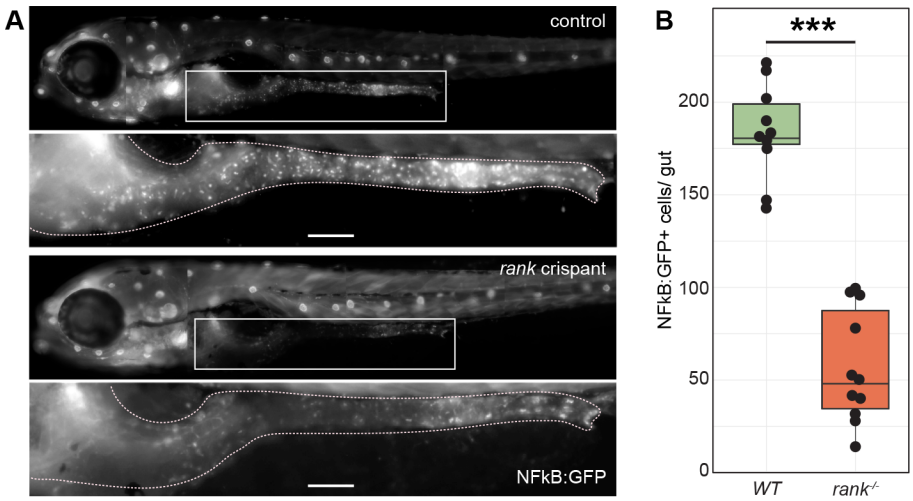

Figure S3. Visualization (A) and quantification (B) of GFP expression in control or *rank* crispant NF-kB:GFP 6 dpf larvae.

Figure S4. Spinal curvature defects in fourteen-week-old *rank* mutant fish relative to wildtype (WT) controls.

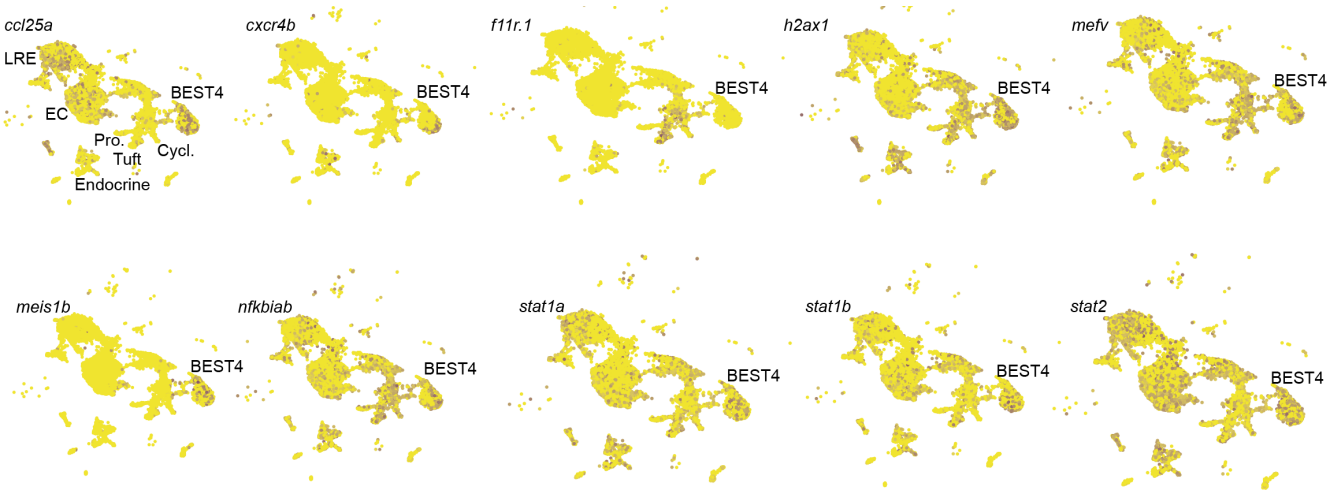

Figure S5. A series of feature plots showing expression of multiple immune regulatory genes in adult intestinal BEST4 cells.

CITATIONS

1. Smillie CS, Biton M, Ordovas-Montanes J, Sullivan KM, Burgin G, Graham DB, et al. Intra- and Inter-cellular Rewiring of the Human Colon during Ulcerative Colitis. Cell. 2019 July 25;178(3):714-730.e22.
2. Parikh K, Antanaviciute A, Fawkner-Corbett D, Jagielowicz M, Aulicino A, Lagerholm C, et al. Colonic epithelial cell diversity in health and inflammatory bowel disease. Nature. 2019 Mar;567(7746):49–55.
3. Feng X, Flüchter P, De Tenorio JC, Schneider C. Tuft cells in the intestine, immunity and beyond. Nat Rev Gastroenterol Hepatol. 2024 Dec;21(12):852–68.
4. Howitt MR, Lavoie S, Michaud M, Blum AM, Tran SV, Weinstock JV, et al. Tuft cells, taste-chemosensory cells, orchestrate parasite type 2 immunity in the gut. Science. 2016 Mar 18;351(6279):1329–33.
5. Gerbe F, Sidot E, Smyth DJ, Ohmoto M, Matsumoto I, Dardalhon V, et al. Intestinal epithelial tuft cells initiate type 2 mucosal immunity to helminth parasites. Nature. 2016 Jan 14;529(7585):226–30.
6. von Moltke J, Ji M, Liang HE, Locksley RM. Tuft-cell-derived IL-25 regulates an intestinal ILC2–epithelial response circuit. Nature. 2016 Jan;529(7585):221–5.
7. Xiong Z, Zhu X, Geng J, Xu Y, Wu R, Li C, et al. Intestinal Tuft-2 cells exert antimicrobial immunity via sensing bacterial metabolite N-undecanoylglycine. Immunity. 2022 Apr 12;55(4):686-700.e7.
8. Eshleman EM, Rice T, Potter C, Waddell A, Hashimoto-Hill S, Woo V, et al. Microbiota-derived butyrate restricts tuft cell differentiation via histone deacetylase 3 to modulate intestinal type 2 immunity. Immunity. 2024 Feb 13;57(2):319-332.e6.
9. Huang L, Bernink JH, Giladi A, Krueger D, van Son GJF, Geurts MH, et al. Tuft cells act as regenerative stem cells in the human intestine. Nature. 2024 Oct;634(8035):929–35.
10. Ono T, Hayashi M, Sasaki F, Nakashima T. RANKL biology: bone metabolism, the immune system, and beyond. Inflamm Regen. 2020 Feb 7;40(1):2.
11. Knoop KA, Kumar N, Butler BR, Sakthivel SK, Taylor RT, Nochi T, et al. RANKL is necessary and sufficient to initiate development of antigen-sampling M cells in the intestinal epithelium. J Immunol Baltim Md 1950. 2009 Nov 1;183(9):5738–47.
12. Nagashima K, Sawa S, Nitta T, Tsutsumi M, Okamura T, Penninger JM, et al. Identification of subepithelial mesenchymal cells that induce IgA and diversify gut microbiota. Nat Immunol. 2017 June;18(6):675–82.
13. Kanaya T, Sakakibara S, Jinnohara T, Hachisuka M, Tachibana N, Hidano S, et al. Development of intestinal M cells and follicle-associated epithelium is regulated by TRAF6-mediated NF-κB signaling. J Exp Med. 2018 Jan 16;215(2):501–19.
14. Onji M, Sigl V, Lendl T, Novatchkova M, Ullate-Agote A, Andersson-Rolf A, et al. RANK drives structured intestinal epithelial expansion during pregnancy. Nature. 2025 Jan;637(8044):156–66.
15. Bando JK, Gilfillan S, Song C, McDonald KG, Huang SCC, Newberry RD, et al. The Tumor Necrosis Factor Superfamily Member RANKL Suppresses Effector Cytokine Production in Group 3 Innate Lymphoid Cells. Immunity. 2018 June 19;48(6):1208-1219.e4.
16. Xu H, Wang Y, Wang W, Fu YX, Qiu J, Shi Y, et al. ILC3s promote intestinal tuft cell hyperplasia and anthelmintic immunity through RANK signaling. Sci Immunol. 2025 May 16;10(107):eadn1491.
17. Wallace KN, Pack M. Unique and conserved aspects of gut development in zebrafish. Dev Biol. 2003 Mar 1;255(1):12–29.
18. Willms RJ, Foley E. Mechanisms of epithelial growth and development in the zebrafish intestine. Biochem Soc Trans. 2023 June 28;51(3):1213–24.
19. Crosnier C, Vargesson N, Gschmeissner S, Ariza-McNaughton L, Morrison A, Lewis J. Delta-Notch signalling controls commitment to a secretory fate in the zebrafish intestine. Dev Camb Engl. 2005 Mar;132(5):1093–104.
20. Wallace KN, Akhter S, Smith EM, Lorent K, Pack M. Intestinal growth and differentiation in zebrafish. Mech Dev. 2005 Feb;122(2):157–73.
21. Rawls JF, Samuel BS, Gordon JI. Gnotobiotic zebrafish reveal evolutionarily conserved responses to the gut microbiota. Proc Natl Acad Sci. 2004 Mar 30;101(13):4596–601.
22. Lickwar CR, Camp JG, Weiser M, Cocchiaro JL, Kingsley DM, Furey TS, et al. Genomic dissection of conserved transcriptional regulation in intestinal epithelial cells. PLoS Biol. 2017 Aug;15(8):e2002054.

23. Willms RJ, Jones LO, Hocking JC, Foley E. A cell atlas of microbe-responsive processes in the zebrafish intestine. Cell Rep. 2022 Feb 1;38(5):110311.
24. Jones LO, Willms RJ, Xu X, Graham RDV, Eklund M, Shin M, et al. Single-cell resolution of the adult zebrafish intestine under conventional conditions and in response to an acute Vibrio cholerae infection. Cell Rep. 2023 Nov 28;42(11):113407.
25. Sato A, Miyoshi S. Fine structure of tuft cells of the main excretory duct epithelium in the rat submandibular gland. Anat Rec. 1997 July;248(3):325–31.
26. Trier JS, Allan CH, Marcial MA, Madara JL. Structural features of the apical and tubulovesicular membranes of rodent small intestinal tuft cells. Anat Rec. 1987 Sept;219(1):69–77.
27. Boyce BF, Xing L. Functions of RANKL/RANK/OPG in bone modeling and remodeling. Arch Biochem Biophys. 2008 May 15;473(2):139–46.
28. ILC3s promote intestinal tuft cell hyperplasia and anthelmintic immunity through RANK signaling [Internet]. [cited 2025 July 29]. Available from: https://www.science.org/doi/10.1126/sciimmunol.adn1491
29. Malonga T, Vialaneix N, Beaumont M. BEST4+ cells in the intestinal epithelium. Am J Physiol-Cell Physiol. 2024 May;326(5):C1345–52.
30. Wen J, Mercado GP, Volland A, Doden HL, Lickwar CR, Crooks T, et al. Fxr signaling and microbial metabolism of bile salts in the zebrafish intestine. Sci Adv. 2021 July 23;7(30):eabg1371.
31. Sur A, Wang Y, Capar P, Margolin G, Prochaska MK, Farrell JA. Single-cell analysis of shared signatures and transcriptional diversity during zebrafish development. Dev Cell. 2023 Dec 18;58(24):3028-3047.e12.
32. Burclaff J, Bliton RJ, Breau KA, Ok MT, Gomez-Martinez I, Ranek JS, et al. A Proximal-to-Distal Survey of Healthy Adult Human Small Intestine and Colon Epithelium by Single-Cell Transcriptomics. Cell Mol Gastroenterol Hepatol. 2022;13(5):1554–89.
33. Wang D, Spoelstra WK, Lin L, Akkerman N, Krueger D, Dayton T, et al. Interferon-responsive intestinal BEST4/CA7+ cells are targets of bacterial diarrheal toxins. Cell Stem Cell. 2025 Apr 3;32(4):598-612.e5.
34. Mitchell KC, Withey JH. Danio rerio as a Native Host Model for Understanding Pathophysiology of Vibrio cholerae. In: Sikora AE, editor. Vibrio Cholerae: Methods and Protocols [Internet]. New York, NY: Springer; 2018 [cited 2025 July 3]. p. 97–102. Available from: https://doi.org/10.1007/978-1-4939-8685-9_9
35. Ito G, Okamoto R, Murano T, Shimizu H, Fujii S, Nakata T, et al. Lineage-specific expression of bestrophin-2 and bestrophin-4 in human intestinal epithelial cells. PloS One. 2013;8(11):e79693.
36. Elmentaite R, Kumasaka N, Roberts K, Fleming A, Dann E, King HW, et al. Cells of the human intestinal tract mapped across space and time. Nature. 2021 Sept;597(7875):250–5.
37. Luna Velez MV, Neikes HK, Snabel RR, Quint Y, Qian C, Martens A, et al. ONECUT2 regulates RANKL-dependent enterocyte and microfold cell differentiation in the small intestine; a multi-omics study. Nucleic Acids Res. 2023 Feb 22;51(3):1277–96.
38. Hernández PP, Strzelecka PM, Athanasiadis EI, Hall D, Robalo AF, Collins CM, et al. Single-cell transcriptional analysis reveals ILC-like cells in zebrafish. Sci Immunol. 2018 Nov 16;3(29):eaau5265.
39. Morales RA, Rabahi S, Diaz OE, Salloum Y, Kern BC, Westling M, et al. Interleukin-10 regulates goblet cell numbers through Notch signaling in the developing zebrafish intestine. Mucosal Immunol. 2022 Aug 1;15(5):940–51.
40. Bottiglione F, Dee CT, Lea R, Zeef LAH, Badrock AP, Wane M, et al. Zebrafish IL-4–like Cytokines and IL-10 Suppress Inflammation but Only IL-10 Is Essential for Gill Homeostasis. J Immunol Author Choice. 2020 Aug 15;205(4):994–1008.
41. O'Leary CE, Ma Z, Culpepper T, Novak SW, DelGiorno KE. New insights into tuft cell formation: Implications for structure–function relationships. Curr Opin Cell Biol. 2022 June 1;76:102082.
42. Angkasekwinai P, Srimanote P, Wang YH, Pootong A, Sakolvaree Y, Pattanapanyasat K, et al. Interleukin-25 (IL-25) Promotes Efficient Protective Immunity against Trichinella spiralis Infection by Enhancing the Antigen-Specific IL-9 Response. Infect Immun. 2013 Oct;81(10):3731–41.
43. Owyang AM, Zaph C, Wilson EH, Guild KJ, McClanahan T, Miller HRP, et al. Interleukin 25 regulates type 2 cytokine-dependent immunity and limits chronic inflammation in the gastrointestinal tract. J Exp Med. 2006 Apr 17;203(4):843–9.

44. Elmentaite R, Kumasaka N, Roberts K, Fleming A, Dann E, King HW, et al. Cells of the human intestinal tract mapped across space and time. Nature. 2021 Sept;597(7875):250–5.
45. Inaba A, Arinaga A, Tanaka K, Endo T, Hayatsu N, Okazaki Y, et al. Interleukin-4 Promotes Tuft Cell Differentiation and Acetylcholine Production in Intestinal Organoids of Non-Human Primate. Int J Mol Sci. 2021 July 24;22(15):7921.
46. Billipp TE, Fung C, Webeck LM, Sargent DB, Gologorsky MB, Chen Z, et al. Tuft cell-derived acetylcholine promotes epithelial chloride secretion and intestinal helminth clearance. Immunity. 2024 June 11;57(6):1243-1259.e8.
47. Ndjim M, Gasmi I, Herbert F, Joséphine C, Bas J, Lamrani A, et al. Tuft cell acetylcholine is released into the gut lumen to promote anti-helminth immunity. Immunity. 2024 June 11;57(6):1260-1273.e7.
48. Wrzosek L, Miquel S, Noordine ML, Bouet S, Chevalier-Curt MJ, Robert V, et al. Bacteroides thetaiotaomicron and Faecalibacterium prausnitziiinfluence the production of mucus glycans and the development of goblet cells in the colonic epithelium of a gnotobiotic model rodent. BMC Biol. 2013 May 21;11(1):61.
49. Troll JV, Hamilton MK, Abel ML, Ganz J, Bates JM, Stephens WZ, et al. Microbiota promote secretory cell determination in the intestinal epithelium by modulating host Notch signaling. Development. 2018 Feb 23;145(4):dev155317.
50. Zagoren E, Dias N, Santos AK, Smith ZD, Ameen NA, Sumigray K. Evidence of secondary Notch signaling within the rat small intestine. Dev Camb Engl. 2025 June 3;152(11):dev204277.
51. de Lau W, Kujala P, Schneeberger K, Middendorp S, Li VSW, Barker N, et al. Peyer's patch M cells derived from Lgr5(+) stem cells require SpiB and are induced by RankL in cultured 'miniguts'. Mol Cell Biol. 2012 Sept;32(18):3639–47.
52. Hickey JW, Becker WR, Nevins SA, Horning A, Perez AE, Zhu C, et al. Organization of the human intestine at single-cell resolution. Nature. 2023 July;619(7970):572–84.
53. Busslinger GA, Weusten BLA, Bogte A, Begthel H, Brosens LAA, Clevers H. Human gastrointestinal epithelia of the esophagus, stomach, and duodenum resolved at single-cell resolution. Cell Rep. 2021 Mar 9;34(10):108819.
54. He XS, Ye WL, Zhang YJ, Yang XQ, Liu F, Wang JR, et al. Oncogenic potential of BEST4 in colorectal cancer via activation of PI3K/Akt signaling. Oncogene. 2022 Feb;41(8):1166–77.
55. Li H, Wang X, Wang Y, Zhang M, Hong F, Wang H, et al. Cross-species single-cell transcriptomic analysis reveals divergence of cell composition and functions in mammalian ileum epithelium. Cell Regen Lond Engl. 2022 May 5;11(1):19.
56. Tang W, Zhong Y, Wei Y, Deng Z, Mao J, Liu J, et al. Ileum tissue single-cell mRNA sequencing elucidates the cellular architecture of pathophysiological changes associated with weaning in piglets. BMC Biol. 2022 May 30;20(1):123.
57. Westfall AK, Gopalan SS, Kay JC, Tippetts TS, Cervantes MB, Lackey K, et al. Single-cell resolution of intestinal regeneration in pythons without crypts illuminates conserved vertebrate regenerative mechanisms. Proc Natl Acad Sci. 2024 Oct 22;121(43):e2405463121.
58. Hoshijima K, Jurynec MJ, Klatt Shaw D, Jacobi AM, Behlke MA, Grunwald DJ. Highly Efficient CRISPR-Cas9-Based Methods for Generating Deletion Mutations and F0 Embryos that Lack Gene Function in Zebrafish. Dev Cell. 2019 Dec 2;51(5):645-657.e4.
59. Schindelin J, Arganda-Carreras I, Frise E, Kaynig V, Longair M, Pietzsch T, et al. Fiji: an open-source platform for biological-image analysis. Nat Methods. 2012 June 28;9(7):676–82.
60. Ewels PA, Peltzer A, Fillinger S, Patel H, Alneberg J, Wilm A, et al. The nf-core framework for community-curated bioinformatics pipelines. Nat Biotechnol. 2020 Mar;38(3):276–8.
61. Patel H, Manning J, Ewels P, Garcia MU, Peltzer A, Hammarén R, et al. nf-core/rnaseq: nf-core/rnaseq v3.19.0 - Tungsten Turtle [Internet]. Zenodo; 2025 [cited 2025 Aug 15]. Available from: https://zenodo.org/records/15631172
62. Patro R, Duggal G, Love MI, Irizarry RA, Kingsford C. Salmon provides fast and bias-aware quantification of transcript expression. Nat Methods. 2017 Apr;14(4):417–9.

63. Love MI, Huber W, Anders S. Moderated estimation of fold change and dispersion for RNA-seq data with DESeq2. Genome Biol. 2014 Dec 5;15(12):550.